fellowship and to the SERC for its continued support of direct methods development at York.

References

DE TITTA, G. T., EDMONDS, J. W., LANGS, D. A. & HAUPTMAN, H. (1975). *Acta Cryst.* A31, 472-479.

GLOVER, I., HANEEF, I., PITTS, J.-E., WOOD, S. P., MOSS, D., TICKLE, I. J. & BLUNDELL, T. L. (1983). *Biopolymers*, 22, 293-304.

HULL, S. E. & IRWIN, M. J. (1978). *Acta Cryst.* A34, 863-870.

KARLE, J. (1968). *Acta Cryst.* B24, 182-186.

WOOLFSON, M. M. & YAO JIA-XING (1988). *Acta Cryst.* A44, 410-413.

Acta Cryst. (1990). A46, 413-422

A Study of the Antisymmetric and Symmetric Parts of the Anharmonic Vibration in Zinc using Synchrotron Radiation

BY GABRIELA KUMPAT AND ELISABETH ROSSMANITH

Mineralogisch-Petrographisches Institut der Universität Hamburg, D-2000 Hamburg, Grindelallee 48, Federal Republic of Germany

(*Received* 30 *October* 1989; *accepted* 11 *December* 1989)

Abstract

The 'almost forbidden' Bragg reflection 061 and the very weak Bragg reflection 0,1,12 of a Zn single-crystal sphere have been carefully analysed to study the antisymmetric and symmetric features of vibrational anharmonicity. The intensity measurements were carried out at room temperature using synchrotron radiation with $\lambda = 0{\cdot}7100\,(3)$ Å taking into account multiple-beam effects. Data recorded on the Hamburger Synchrotronstrahlungslabor (HASYLAB) are discussed in terms of the anharmonic atomic vibrations using the effective one-particle-potential formalism. The outcome concerning third- and fourth-order anharmonicity is in accordance with previous results of the authors derived by least-squares fitting of measured Bragg intensities and disprove results given by Merisalo & Larsen [*Acta Cryst.* (1979) A35, 325-327] and Merisalo, Järvinen & Kurittu [*Phys. Scr.* (1978), 17, 23-25]. The measured very weak intensity of the almost forbidden 061 reflection can be well interpreted in terms of a small but significant antisymmetric anharmonic thermal motion of the Zn atoms characterized by the third-order anharmonic temperature parameter $\alpha_{33} = -0{\cdot}16\,(2) \times 10^{-19}$ J Å^{-3}.

Introduction

The conditions limiting possible reflections for special atomic positions in the unit cell, as given in *International Tables for X-ray Crystallography* (1974), are correct only in the case of centrosymmetric scattering centres. In conventional structure analysis the assumption is made that the electron distribution of an atom has spherical symmetry. The Bragg reflections not matching the conditions limiting possible reflections are supposed therefore to have zero intensity. In general, however, crystal atoms are not expected to be spherically symmetric, and therefore such reflections are not strictly forbidden.

The deviations from spherical symmetry of the atomic electron cloud can be due to static directional distortions of the electronic charge distribution associated with chemical bonding in the structure as well as with the dynamic asphericity associated with anharmonic temperature vibration. Because asphericity due to chemical bonding mainly affects the Bragg intensity of the low-order reflections, the effect of anharmonic motion can usually be separated by a measurement at high values of the scattering vector **h** where the effects of bonding can be ignored.

In Dawson's structure-factor formalism (Dawson, 1967) the deviations from spherical symmetry of the atomic electron cloud is taken into consideration by replacing the spherical atomic electron densities of the atoms by vibration-modified aspherical densities ρ_j' given as the convolution of the aspherical at-rest distribution ρ_j and the aspherical nuclear thermal smearing function t_j:

$$\rho_j' = (\rho_c + \rho_a)_j * (t_c + t_a)_j, \qquad (1)$$

where the subscripts c and a denote the parts of ρ and t which possess centrosymmetry and antisymmetry, respectively, about the nuclear positions r_j of the atoms j in the unit cell.

The Fourier-transform relation between the structure factor and the electron density of the crystal is then given by

$$F(\mathbf{h}) = \sum f_j(\mathbf{h})\, T_j(\mathbf{h}) \exp(2\pi i \mathbf{h} \mathbf{r}_j) = A(\mathbf{h}) + iB(\mathbf{h}), \qquad (2)$$

where the transforms of ρ_j and t_j, the atomic scattering factor f_j and the temperature factor T_j, are both

0108-7673/90/050413-10$03.00

complex quantities:

$$f_j(\mathbf{h}) = f_j(\mathbf{h})_c + if_j(\mathbf{h})_a \quad (3)$$

$$T_j(\mathbf{h}) = T_j(\mathbf{h})_c + iT_j(\mathbf{h})_a. \quad (4)$$

For the case of the hexagonal closed-packed structure of Zn (space group $P6_3/mmc$) with two atoms in the unit cell at the special positions $\pm(\frac{1}{3}, \frac{2}{3}, \frac{1}{4})$ with site symmetry $\bar{6}m2$ and the origin at the centre $\bar{3}m1$ the antisymmetric parts f_a and T_a of the two atoms are related by inversion:

$$f_a(\tfrac{1}{3}, \tfrac{2}{3}, \tfrac{1}{4}) = -f_a(-\tfrac{1}{3}, -\tfrac{2}{3}, -\tfrac{1}{4})$$

$$T_a(\tfrac{1}{3}, \tfrac{2}{3}, \tfrac{1}{4}) = -T_a(-\tfrac{1}{3}, -\tfrac{2}{3}, -\tfrac{1}{4})$$

and must reflect the site symmetry of the atomic position. With

$$f_c(\tfrac{1}{3}, \tfrac{2}{3}, \tfrac{1}{4}) = f_c(-\tfrac{1}{3}, -\tfrac{2}{3}, -\tfrac{1}{4})$$

$$T_c(\tfrac{1}{3}, \tfrac{2}{3}, \tfrac{1}{4}) = T_c(-\tfrac{1}{3}, -\tfrac{2}{3}, -\tfrac{1}{4})$$

and

$$a = 2\cos 2\pi[(h+2k)/3 + l/4] \quad (5a)$$

$$b = 2\sin 2\pi[(h+2k)/3 + l/4], \quad (5b)$$

in the case of Zn (2) reduces to

$$F(\mathbf{h}) = af_c(\mathbf{h})T_c(\mathbf{h}) - af_a(\mathbf{h})T_a(\mathbf{h}) - bf_c(\mathbf{h})T_a(\mathbf{h}) - bf_a(\mathbf{h})T_c(\mathbf{h}). \quad (6)$$

Because of the space-group symmetry, the reflections with $h = k$ and $l =$ odd are strictly forbidden. For these reflections a, defined in (5a), is zero and f_a and T_a vanish by symmetry.

The structure factor for the almost forbidden reflections with $h+2k = 3n$ ($h \neq k$) and $l =$ odd, where a, defined in (5a), is likewise zero, depends on the antisymmetric parts of the atomic scattering factor and temperature factor only:

$$F(\mathbf{h}) = -b[f_c(\mathbf{h})T_a(\mathbf{h}) + f_a(\mathbf{h})T_c(\mathbf{h})]. \quad (7)$$

The corresponding intensity is therefore expected to be very weak.

With the assumption that f_a is zero for large scattering vectors $\mathbf{h}$, the structure factor of Zn for the almost forbidden high-order reflections reduces to

$$F(\mathbf{h})_1 = 2f_c(\mathbf{h})T_a(\mathbf{h}). \quad (8)$$

On the other hand, the structure factor of the reflections with $h+2k = 3n$ and $l =$ even and large scattering vectors $\mathbf{h}$ depends solely on the centrosymmetric part of T_c:

$$F(\mathbf{h})_2 = 2f_c(\mathbf{h})T_c(\mathbf{h}). \quad (9)$$

For all other reflections, both centrosymmetric and antisymmetric terms of T_j are present in the structure factor of Zn:

$$F(\mathbf{h})_3 = f_c(aT_c - bT_c), \quad (10)$$

where a and b can take the values ± 1 and $\pm 1{\cdot}732$.

Previous work on anharmonicity in Zn

An X-ray study on Bragg intensity measurements of the 'almost forbidden' reflections 301 and 303 in a Zn crystal performed with Mo $K\alpha$ radiation has been reported by Merisalo, Järvinen & Kurittu (1978) (M, J & K hereafter). They discussed their results in terms of the anharmonic atomic vibrations using the effective one-particle-potential (OPP) formalism developed by Dawson and Willis (Willis & Pryor, 1975). The expression for the anharmonic temperature factor used by M, J & K for Zn has been derived by Merisalo & Larsen (1977) (M & L 77 hereafter). Having regard to the site symmetry of the Zn atoms, they expanded the potential $V(\mathbf{u})$, experienced by the atom under small displacements from the equilibrium position in the crystal, $\mathbf{u}$, in a power series as a function of the Cartesian coordinates u_x, u_y, u_z of $\mathbf{u}$, where terms up to fourth order were retained. The definition of the Cartesian-coordinate system with respect to the lattice vectors $\mathbf{a}$, $\mathbf{b}$, $\mathbf{c}$ is shown in Fig. 1. Because of the site symmetry of the Zn atom in the h.c.p. lattice the number of second-order (harmonic) parameters reduces to two (α_{20}, β_{00}), the number of third-order parameters reduces to one (α_{33}) and the number of fourth-order parameters reduces to three ($\alpha_{40}, \beta_{20}, \gamma_{00}$). In the classical regime, the thermal smearing function t_j (sometimes called probability density function p.d.f.) of an atom is obtained from the potential according to the Boltzmann distribution:

$$t_j = \exp[-V(\mathbf{u})/k_BT]/Z, \quad (11a)$$

where Z is the partition function, k_B the Boltzmann constant and T the absolute temperature. Because the Fourier transform of the anharmonic thermal

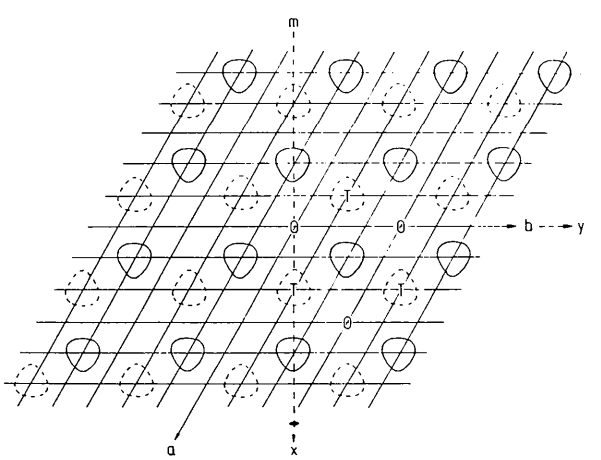

Fig. 1. A basal projection of the atomic arrangement of Zn and definition of the Cartesian coordinate system with respect to the lattice vectors. Equipotential contours are exaggerately represented. Solid line for $z = \frac{1}{4}$ (α_{33} negative), dashed line for $z = -\frac{1}{4}$ (α_{33} positive). O: Octahedral hole, T: tetrahedral hole.

Table 1. *Previous work: harmonic and anharmonic parameters for the* Zn *atom in the special position* $\frac{1}{3}, \frac{2}{3}, \frac{1}{4}$

	M, J & K X-rays, Mo $K\alpha$	M & L 79 Neutrons, 1·070 Å	Rossmanith *et al.* (1990) X-rays, Mo $K\alpha$
$\alpha_{20}(10^{-19}\,\text{J Å}^{-2})$	—	−1·109 (10)	−0·815 (4)
$\beta_{00}(10^{-19}\,\text{J Å}^{-2})$	—	1·841 (10)	1·613 (6)
$\alpha_{33}(10^{-19}\,\text{J Å}^{-3})$	−1·5 (3)	−1·80 (30)	−0·181 (72)
$\alpha_{40}(10^{-19}\,\text{J Å}^{-4})$	—	0·25 (28)	0·352 (144)
$\beta_{20}(10^{-19}\,\text{J Å}^{-4})$	—	7·36 (28)	−0·301 (137)
$\gamma_{00}(10^{-19}\,\text{J Å}^{-4})$	—	−6·27 (14)	0·129 (74)
$V = 0{\cdot}02\times10^{-19}$ J			
$\lvert u_{+x}\rvert$ (Å)	—	0·0957 (7)	0·1009 (2)
$\lvert u_{-x}\rvert$ (Å)	—	0·0893 (5)	0·1000 (2)
$V = 0{\cdot}08\times10^{-19}$ J			
$\lvert u_{+x}\rvert$ (Å)	—	0·2001 (33)	0·2027 (8)
$\lvert u_{-x}\rvert$ (Å)	—	0·1734 (16)	0·1991 (7)
$V = 0{\cdot}18\times10^{-19}$ J			
$\lvert u_{+x}\rvert$ (Å)	—	0·3169 (99)	0·3056 (18)
$\lvert u_{-x}\rvert$ (Å)	—	0·2535 (32)	0·2974 (16)
$\langle u_a^2\rangle_{\text{harm}}^{1/2}$ (Å)	—	0·092 (3)	0·1005 (2)
$\langle u_c^2\rangle_{\text{harm}}^{1/2}$ (Å)	—	0·166 (4)	0·1595 (2)
$\langle u_a^2\rangle_{\text{anharm}}^{1/2}$ (Å)	—	0·106 (2)*	0·1004 (2)
$\langle u_c^2\rangle_{\text{anharm}}^{1/2}$ (Å)	—	0·161 (2)*	0·1591 (2)

* Given by M & L 79, calculated using a truncated expansion of the Boltzmann distribution function instead of (11).

smearing function cannot be written as a closed algebraic expression, the anharmonic part of t_j is expanded into series to make analytical integration, *i.e.* Fourier transformation, possible:

$$t_j = \{\exp[-V(\mathbf{u})_{\text{harm}}/(k_BT)] \times [1 - V(\mathbf{u})_{\text{anharm}}/(k_BT)]\}/Z'. \quad (11b)$$

$V(\mathbf{u})_{\text{harm}}$ and $V(\mathbf{u})_{\text{anharm}}$ are the harmonic and anharmonic parts of the potential and Z' is the corresponding partition function. The antisymmetric and symmetric parts T_a and T_c of $T_j(\mathbf{h})$ can then be given as functions of the third- and fourth-order anharmonic parameters respectively:

$$T_a(\mathbf{h}) = T_{\text{harm}}(\mathbf{h})4(a^*\pi)^3(k_BT)^2 \times [\alpha_{33}/N(2\beta_{00}-\alpha_{20})^3](h-k) \times (2h^2+2k^2+5hk), \quad (12)$$

where a^* is the reciprocal-lattice constant in the basal plane, T_{harm} is the harmonic temperature factor. The normalization factor N and the somewhat lengthy expression for $T_j(\mathbf{h})_c$ are given in M & L 77 in full and will not be repeated here.

The result for the third-order anharmonic parameter α_{33} reported by M, J & K is given in Table 1 together with results for the third- and fourth-order anharmonic parameters obtained from least-squares fit of a Bragg intensity data set measured with neutrons ($\lambda = 1{\cdot}070$ Å) by Merisalo & Larsen (1979) (M & L 79 hereafter) and from least-squares-fit results of a Bragg intensity data set of a Zn single-crystal sphere with radius 46 μm, measured with Mo $K\alpha$ radiation by the authors (to be published). The harmonic parameters α_{20} and β_{00} used by the authors in the refinement of the anharmonic parameters are derived from the conventional anisotropic harmonic temperature coefficients β_{11} and β_{33} using the relations

$$\beta_{00} = (\pi^2k_BT/3)(2a^{*2}/\beta_{11} + c^{*2}/\beta_{33}) \quad (13a)$$

$$\alpha_{20} = (2\pi^2k_BT/3)(-a^{*2}/\beta_{11} + c^{*2}/\beta_{33}), \quad (13b)$$

where c^* is the reciprocal-lattice constant normal to the basal plane.

Because of the strong correlation between the anharmonic and harmonic parameters, the latter were not refined simultaneously with the anharmonic ones. The β_{11} and β_{33} used for calculation of the α_{20} and β_{00} are the result of the purely harmonic refinement of the same data set. The root-mean-square displacements in the **a** and **c** directions of the lattice, calculated using the relations

$$(\langle u_a^2\rangle_{\text{harm}})^{1/2} = [\beta_{11}/(2\pi^2a^{*2})]^{1/2} = [k_BT/(2\beta_{00}-\alpha_{20})]^{1/2} \quad (14a)$$

and

$$(\langle u_c^2\rangle_{\text{harm}})^{1/2} = [\beta_{33}/(2\pi^2c^{*2})]^{1/2} = \{k_BT/[2(\beta_{00}+\alpha_{20})]\}^{1/2} \quad (14b)$$

are also given in Table 1.

A non-zero value of the third-order anharmonic temperature parameter α_{33} implies a deviation from centrosymmetry of the thermal vibration of the Zn atoms as exaggeratedly shown in Fig. 1. This deviation is consistent with the site symmetry $\bar{6}m2$ of the special position. For negative α_{33}, the potential expanded to third order (see M & L 77)

$$V(\mathbf{u}) = V_0 + V_{\text{harm}} + \alpha_{33}(u_x^3 - 3u_xu_y^2) \quad (15a)$$

is softened in the x direction and hardened in the opposite direction (Fig. 1). V_0 is arbitrarily set to zero and the harmonic part of the potential is given by

$$V_{\text{harm}} = (\beta_{00}-\alpha_{20}/2)(u_x^2+u_y^2) + (\beta_{00}+\alpha_{20})u_z^2. \quad (15b)$$

The values for **u** in the **x** and **−x** directions, calculated for $V(\mathbf{u}) = 0{\cdot}02$, $0{\cdot}08$ and $0{\cdot}18\times10^{-19}$ J, the potentials which correspond to the harmonic potential in the basal plane, inserting in (15*b*) the onefold, twofold and threefold root-mean-square displacement $\langle u_a^2\rangle^{1/2}$, are also given in Table 1. The deviations from centrosymmetry for these potential values are about 3·2, 6·0 and 8·4% respectively in the **−x** and 3·8, 8·5 and 14·6% in the **+x** directions for M & L 79 data and 0·45 (0·88, 1·30) and 0·46% (0·92, 1·39%) respectively for the authors' data.

The value determined for α_{33} by M & L 79 as well as by the authors is negative for the atom in the position $\frac{1}{3}, \frac{2}{3}, \frac{1}{4}$ and positive for the position $-\frac{1}{3}, -\frac{2}{3},$

$-\frac{1}{4}$. This result can be interpreted quite reasonably as enlargement of the amplitudes of vibration towards the side with octahedral holes and reduction towards the side with tetrahedral holes (Fig. 1) and is therefore physically meaningful.

It is not possible to determine the sign of α_{33} from intensity measurement of 'almost forbidden' reflections. M, L & K therefore adopted the negative sign from the above-mentioned reasoning.

The effect of the third- as well as the fourth-order parameters can be discussed by inspection of the root-mean-square amplitudes of the atomic vibrations in the principal directions, evaluated in the high-temperature limit as an ensemble average by the Boltzmann distribution function

$$(\langle u_i^2\rangle_{\text{anharm}})^{1/2} = \int u_i^2 t \, dv / \int t \, dv; \quad i = \mathbf{a}, \mathbf{c}. \quad (14c)$$

These values are also given in Table 1. Whereas the anharmonic parameters given by M & L 79 indicate a considerable increase of the mean-square amplitude in the basal plane, the integral effect of anharmonicity determined by the authors is negligibly small.

Apart from the physically significant sign of the third-order parameter, the anharmonic parameters given by M & L 79 and M, J & K and those given by the authors differ appreciably. A redetermination of the third-order parameter from the intensity measurement of an 'almost forbidden' reflexion seemed therefore to be valuable and necessary.

Experimental

To find the most favourable experimental conditions for this measurement, the values of the relativistic Hartree–Fock atomic scattering factors of Zn^{2+} for the 'almost forbidden' reflections with $(\sin\theta)/\lambda < 1{\cdot}4$ Å^{-1} were collated in Table 2(a) together with the antisymmetric part of the temperature factor. The values for T_a in the fourth column of Table 2(a) were obtained by inserting in (12) the anharmonic temperature parameters given by M & L 79. The absolute value of the structure factor calculated from (8) is given in the fifth column. The structure factors obtained using the anharmonic temperature parameters given by the authors (Table 1) are about one sixth of the values given in Table 2(a).

Because the antisymmetric part of the temperature factor T_a has its maximum for $(\sin\theta)/\lambda \sim 1{\cdot}3$ Å^{-1}, the 601 reflection is expected to be the most intense 'almost forbidden' reflection. The estimated relative integrated intensities

$$I_{\text{rel}} = F(\mathbf{h})^2 * \text{Lp} * 1500/A \quad (16a)$$

for a Zn single-crystal sphere with radius = 100 μm and a linear absorption coefficient $\mu_0 = 395{\cdot}7$ cm^{-1} are given in the sixth column of Table 2(a). A is the absorption factor for spheres from Weber (1969) and

Table 2. *Expected relative integrated intensities of the 'almost forbidden' reflections of a* Zn *single crystal sphere with radius* 100 μm *and* $\lambda = 0{\cdot}71$ Å

(a) Estimated using M & L 79 anharmonic parameters

h	k	l	$(\sin\theta)/\lambda$ (Å^{-1})	f_c	T_a	F_c	I_{rel}
3	0	1	0·66	11·1	0·009	0·21	2·26
3	0	3	0·72	10·2	0·008	0·16	1·37
3	0	5	0·82	8·9	0·005	0·10	0·55
3	0	7	0·96	7·7	0·003	0·05	0·16
1	4	1	1·00	7·4	0·019	0·28	5·84
1	4	3	1·04	7·2	0·016	0·23	4·07
1	4	5	1·12	6·8	0·011	0·15	2·04
3	0	9	1·12	6·8	0·002	0·02	0·04
1	4	7	1·22	6·4	0·007	0·08	0·80
3	0	11	1·29	6·1	0·001	0·01	0·01
6	0	1	1·30	6·1	0·032	0·39	24·64
6	0	3	1·34	6·0	0·027	0·32	20·35
1	4	9	1·35	5·9	0·003	0·04	0·32
2	5	1	1·36	5·9	0·022	0·26	16·18
2	5	3	1·39	5·8	0·018	0·21	17·49
6	0	5	1·40	5·8	0·018	0·21	23·51

(b) Comparison of the expected relative integrated intensities (authors' harmonic parameters) with measured ones, $\lambda = 0{\cdot}71$ Å. I: measured integrated intensities; I_{Bg}: measured background intensity; S: defined in (16c)

h	k	l	$(\sin\theta)/\lambda$ (Å^{-1})	f_c	F_{harm}	I_{rel}	IS CAD-4 (counts s^{-1})	$I_{\text{BG}}S$ CAD-4 (counts s^{-1})	IS Synchrotron (counts s^{-1})	$I_{\text{BG}}S$ Synchrotron (counts s^{-1})
0	1	12	1·24	6·3	0·32	12	0·6 (3)	9·8 (3)	11 (1)	52 (1)
6	0	2	1·32	6·1	2·89	1489	35·5 (6)	17·8 (4)	1456 (4)	70 (1)

the Lorentz–polarization factor Lp is calculated using

$$\text{Lp} = 0{\cdot}5 * [(1+\text{DP}) + (1-\text{DP}) * \cos^2 2\theta]/\sin 2\theta \quad (16b)$$

where θ is the Bragg angle for Mo $K\alpha$ radiation and DP = 0·90 is the degree of polarization of the incident beam.

For comparison the relative integrated intensities of the 602 and 0,1,12 reflection, calculated in the harmonic approximation using the parameters estimated by the authors, are given in Table 2(b), together with the integrated intensities measured with Mo $K\alpha$ radiation on the single-crystal CAD-4 diffractometer by Enraf–Nonius.

If one bears in mind the peak broadening for high-order reflections due to the $K\alpha_1$ and $K\alpha_2$ lines as well as the divergence of the incident beam, inspection of the data given in Tables 2(a) and (b) explains why the trial of the authors to measure the intensities of 'almost forbidden' reflections of the Zn single-crystal sphere using a conventional Mo $K\alpha$ tube miscarried. This fact is even more understandable taking into consideration that the expected intensities in Table 2(a) would be considerably reduced if the anharmonic parameters obtained by the authors were used for calculation.

On the other hand, because of the small divergence and the high intensity of the incident beam, synchrotron radiation is a very well suited tool for measurements of very weak high-order reflections, as

can be seen from Fig. 2(*a*), in which the ω–2θ scan of the high-order $\bar{1}\bar{4}6$ reflection measured with synchrotron radiation is compared with the ω–2θ scan measured with the CAD-4 (Fig. 2*b*). The integrated intensities of the 061 and 0,1,12 reflections, measured with synchrotron radiation, also given in Table 2(*b*), confirm this fact.

Assuming the validity of the M & L 79 anharmonic parameters, the integrated intensity of the 'almost forbidden' 061 reflection is expected to be twice as large as the intensity of the 0,1,12 reflection. A well resolved peak should therefore be observable when using synchrotron radiation for the measurement of this Bragg reflection.

The electron-storage ring DORIS II at the Hamburger Synchrotronstrahlungslabor (HASYLAB) of the Deutsches Elektronensynchrotron (DESY, Hamburg, FRG) provides a continuous X-ray spectrum in the energy region from several eV up to several 100 keV, when operated with 3·7 GeV. The ring current decreased from about 100 to 30 mA in 4 h cycles during the measurements. The experiment was performed on beam line *C*. The vertical divergence of the synchrotron radiation at this beam line was calculated to be 70 μrad with a brightness of about 2×10^{13} photons (mrad^2 s 0·1%BW)$^{-1}$. A flat double Ge(111) perfect-crystal monochromator was used to select the 17·465 keV energy [=0·7100 (3) Å]. Since 222 is an 'almost forbidden' reflection in Ge, the $\lambda/2$ content in the incident beam is negligible. Higher-order harmonics can be ignored because of their small content in the spectral distribution of the synchrotron radiation impinging on the monochromator and because of the possibility to greatly attenuate possible contents by deliberately offsetting the Bragg angle of the second Ge monochromator crystal. Moreover, the final detector, an NaI proportional counter, clearly separates the fundamental from the possibly remaining harmonics. The beam size used in the experiment was about 0·4 mm horizontal and 0·4 mm vertical at the sample position. A monitor device, consisting of a Kapton scatterer in the beam between the monochromator and the sample and an NaI scintillation counter mounted below the Kapton foil, enables the continuous real-time monitoring of the fluctuating primary-beam intensity during the experiment. Depending on the ring current, a monitor intensity between 40 000 and 10 000 counts s^{-1} was detected. For standardization of the intensity of the diffractometer detector a factor

$$S = 30\,000/I_m \qquad (16c)$$

was used, where I_m is the real-time dead-time-corrected monitor intensity.

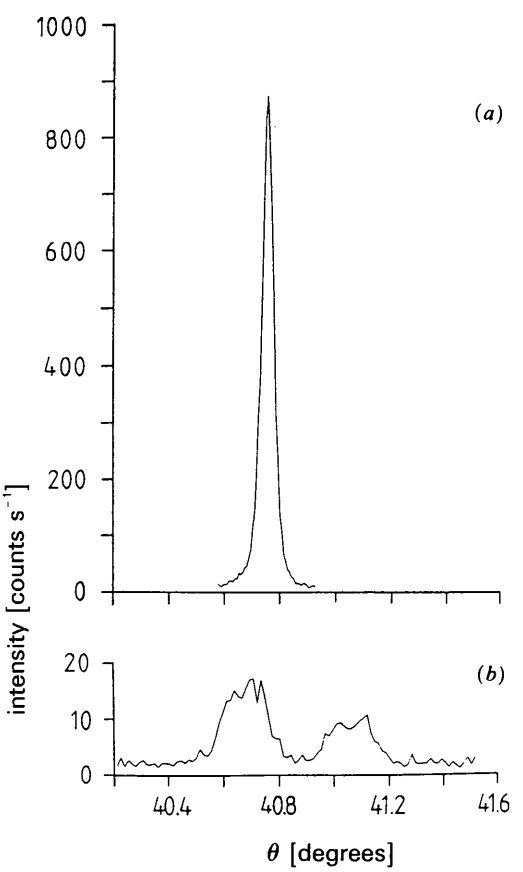

Fig. 2. ω–2θ scan of the $\bar{1}\bar{4}6$ reflection, Zn sphere with radius 46 μm. Bragg intensity in counts s^{-1}. (*a*) Measured with synchrotron radiation, λ = 0·5607 (3) Å, intensity not standardized, ring current about 50 mA, total counting time = 150 s. (*b*) Measured with CAD-4, Ag $K\alpha$, total counting time 600 s.

The single-crystal sphere [99·9999% Zn, diameter = 200 μm, unit-cell dimensions $a = b = 2{\cdot}6654\,(4)$, $c = 4{\cdot}9423\,(3)$ Å] was mounted on the ψ-(6-)circle diffractomer (Hümmer, Weckert & Bondza, 1989). Since the synchrotron radiation is linearly polarized in the horizontal plane, the intensities of the 602 reflection, the very weak 0,1,12 reflection and the 'almost forbidden' 061 reflection were measured in the vertical diffraction plane. The 602 reflection, which does not depend on the antisymmetric part of the temperature parameter [(9)], was therefore well suited for scaling of the measured structure factors of the 0,1,12 and 061 reflections. The integrated intensity of the 0,1,12 reflection was not only used as a measure for the observability of the 'almost forbidden' reflections, but it was also of interest because of the considerable sensitivity of its calculated structure factor [(10)] on the third- as well as on the fourth-order anharmonic parameters. The integrated intensities of the 602 and 0,1,12 reflection were measured using the ω–2θ step-scanning technique. To avoid intensity contributions due to multiple diffraction, in both cases the crystal was rotated about the reflection-plane normal in an azimuthal angle range free from multiple-scattering events. This ψ range was calculated before measurement using the programs *UMWEG* (Rossmanith, 1985) and

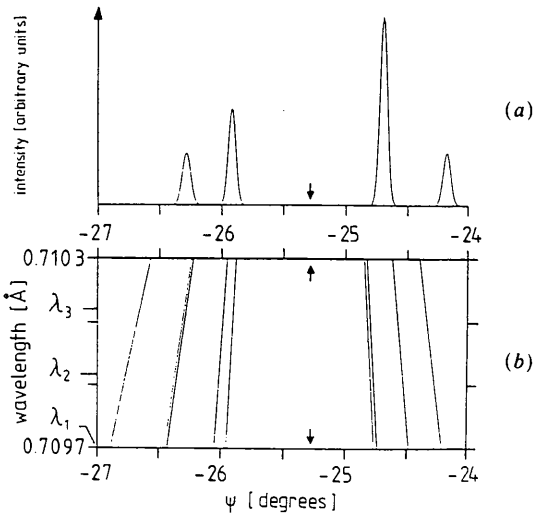

Fig. 3. *Umweganregung*-peak-location plots and ψ-scan simulations for the 0,1,12 reflection. Peak-broadening parameter $\varepsilon = 0{\cdot}0005$ Å; the ψ value used in the measurement is indicated by an arrow. (*a*) ψ-scan simulation for $\lambda = 0{\cdot}7099$ Å; (*b*) ψ-λ diagram, λ_1, λ_2 and λ_3 are the wavelengths deduced from the different Bragg positions observed (see Fig. 5 and text).

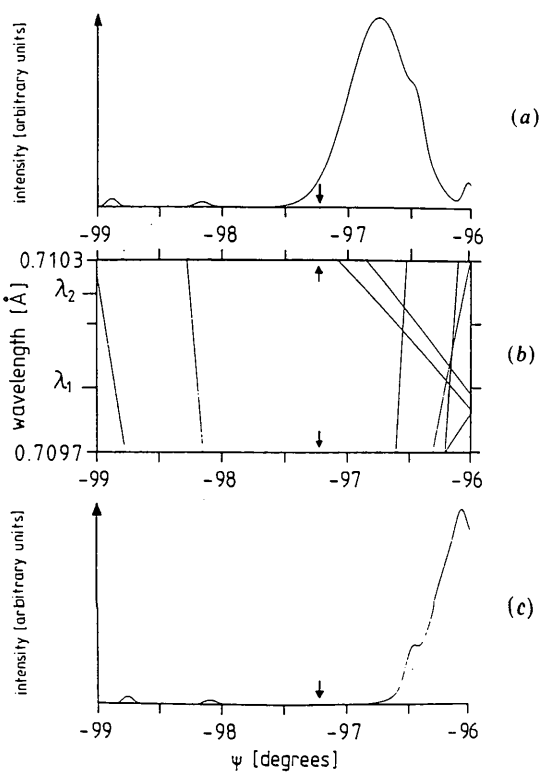

Fig. 4. *Umweganregung*-peak-location plots and ψ-scan simulations for the 602 reflection. Peak-broadening parameter $\varepsilon = 0{\cdot}0005$ Å. (*a*) ψ-scan simulation for $\lambda_2 = 0{\cdot}7102$ Å; (*b*) ψ-λ diagram, λ_1 and λ_2 are the wavelengths deduced from the different Bragg positions observed; (*c*) ψ-scan simulation for $\lambda_1 = 0{\cdot}7099$ Å.

PSILAM (Rossmanith, Kumpat & Schulz, 1990). In Figs. 3 and 4 the ψ-λ diagrams and the computer simulations of the *Umweganregung* patterns of these regions for both reflections are given. For the peak-broadening parameter ε (Rossmanith, 1985) the value $0{\cdot}0005$ Å^{-1}, deduced from previous experience with the Zn sample, was used. The ψ values adjusted in the measurements of the integrated intensities are indicated by an arrow. Both reflections were measured before and after the measurement of the 'almost forbidden' 061 reflection. For both reflections a range of 1° in ω was scanned. The step width in ω and the counting time per step were 0·006° and 3 s respectively for the 0,1,12 reflection and 0·007° and 1 s for the 602 reflection. In Fig. 5 the measured standardized intensity profiles of the 0,1,12 reflection are shown. The small fluctuation in the position of the Bragg

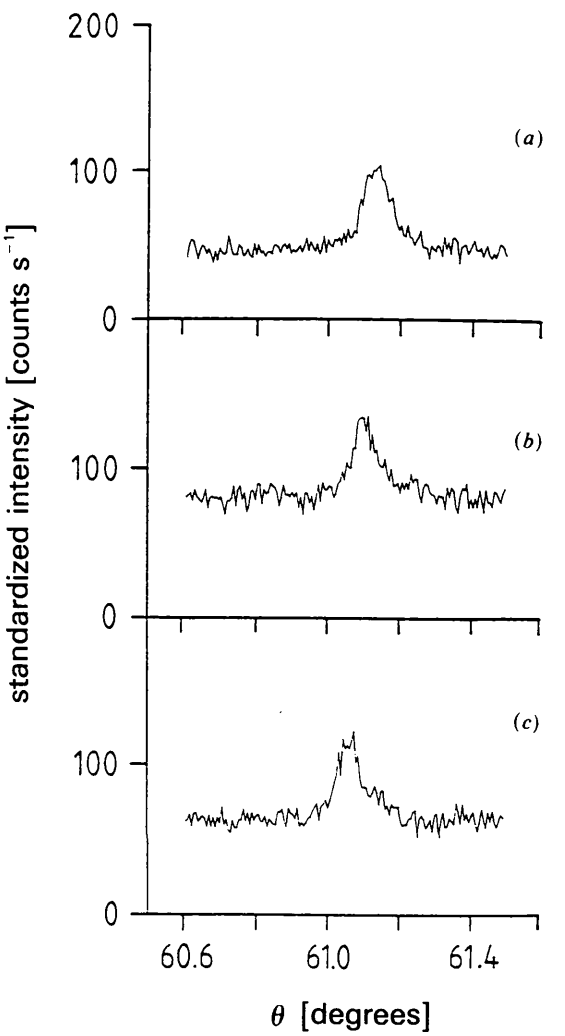

Fig. 5. The ω-2θ scans of the 0,1,12 reflection. Standardized intensity in counts s^{-1} *versus* ω. Estimation of the wavelength fluctuation from the position of the Bragg-peak maxima: (*a*) $\theta = 61{\cdot}13° \equiv \lambda_3 = 0{\cdot}7101$ Å; (*b*) $\theta = 61{\cdot}10° \equiv \lambda_2 = 0{\cdot}7099$ Å; (*c*) $\theta = 61{\cdot}07° \equiv \lambda_1 = 0{\cdot}7097$ Å.

angle is probably due to the instability of the beam of the synchrotron-radiation source impinging on the monochromator and the fluctuation of the wavelength resulting therefrom. Whereas the azimuthal region free from multiple scattering events is nearly constant for the wavelengths deduced from the different Bragg positions observed in the case of the 0,1,12 reflection (Fig. 3*b*), in the case of the 602 reflection the Bragg intensity of the second measurement may be influenced by *Umweganregung* events of the upper part of Fig. 4(*b*) because of the wideness of the lines involved (Fig. 4*a*). This result demonstrates once more (see Rossmanith, Kumpat & Schulz, 1990) the necessity not only to check the absence of multiple scattering events with the help of an appropriate ψ–λ diagram, but also to determine the width of the lines in the vicinity of the ψ position used in the measurement.

To ensure that no multiple Bragg events made a contribution to the measured intensity of the 'almost forbidden' 061 reflection, the integrated intensity of this reflection was measured using the ω–2θ–ψ scanning technique (Rossmanith, 1986). This technique was necessary because of the above-mentioned instability of the wavelength of the synchrotron radiation. Furthermore with this technique it was possible to check the reproducibility of the angular settings of the ω, χ and φ circles of the diffractometer during measuring time. Since the ψ circle of the diffractometer acts only in the horizontal diffraction plane, in our experiment the ψ scan, *i.e.* the rotation about the diffraction vector, had to be achieved by a combined rotation about the φ, χ and ω axes of the diffractometer. For each azimuthal angle ψ the diffractometer setting angles φ, χ and ω were calculated with the diffractometer-control program *MONI* by Weckert (1988) using formulae as given, for example, by Busing & Levy (1967). The measurement was performed in the azimuthal angle range, whose ψ-scan simulation, calculated with the program *UMWEG*, is shown in Fig. 6(*a*). For one hundred steps per degree in ψ the intensity was measured in

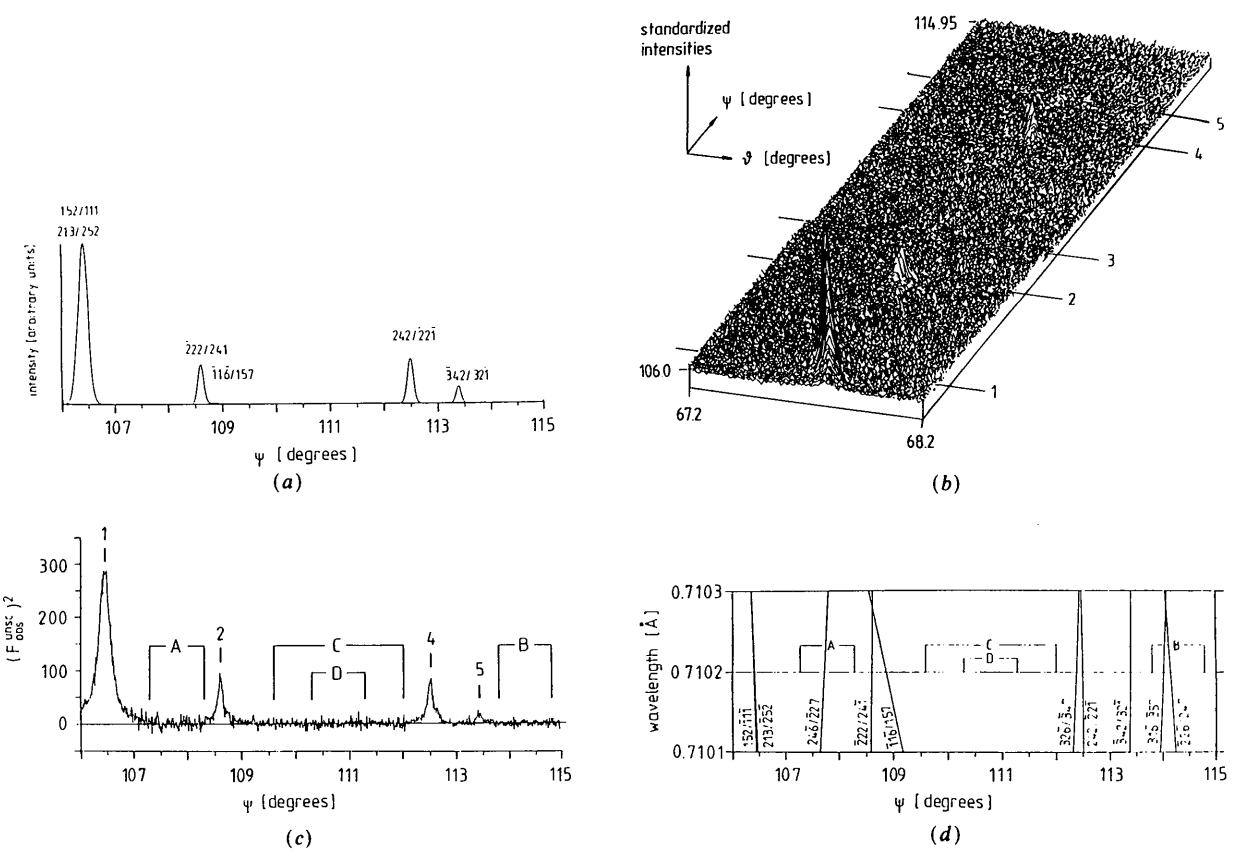

Fig. 6. (*a*) ψ-scan simulation for the 601 reflection. *hkl* of the operative/cooperative reflections are given. Peak-broadening parameter $\varepsilon = 0{\cdot}0005$ Å^{-1}, $\lambda = 0{\cdot}71020$ Å. (*b*) 3D plot of the ω–2θ–ψ scan: standardized intensity *versus* θ and ψ. ψ position 1: *Umweganregung* event used as reference intensity; ψ positions 2, 4 and 5: positions of the peak maxima of the *Umweganregung* events; ψ position 3: position at which attempts for background reduction were made. (*c*) Integrated intensity *versus* ψ. To enable comparison with the unscaled observed structure factors given in Table 3, the integrated intensity is multiplied by $A/[\mathrm{Lp}(1+\alpha_{\mathrm{TDS}})]$. *A*–*D*: regions used for evaluation of $F_o(061)$. (*d*) ψ–λ diagram for the 061 reflection, horizontal line: $\lambda = 0{\cdot}7102$ Å according to $\theta_{\max}(061)$ of the measured *Umweganregung* peaks. *hkl* of the operative/cooperative reflections are given. *A*–*D*: regions used for evaluation of $F_o(061)$.

ω–2θ scans consisting of 102 steps with 0·01° step length in ω and 1 s counting time per step. The well resolved *Umweganregung*-peak intensity at the maximum of the first multiple reflection in Fig. 6(*a*) was measured as reference after each new injection of the storage ring to ensure the reproducibility of the experimental conditions. Because no significant integrated intensity could be observed in the azimuthal range free from multiple-scattering events, the ω–2θ–ψ scanning was interrupted and attempts were made to reduce the relatively high background intensity (not standardized background intensity $I_{Bg} = 110$ counts s^{-1} for ring current = 100 mA). The background was halved by collimation of the incident and reflected beam and by shielding the NaI detector with a lead foil.

Results and discussion

In Fig. 6(*b*) a 3D plot of the measured ω–2θ–ψ scan is given. The standardized intensity is plotted *versus* ω and ψ. For each step in ψ of this scan the integrated intensity was calculated and plotted against ψ in Fig. 6(*c*), showing the excellent agreement with the computed ψ-scan simulation of Fig. 6(*a*) and hence demonstrating the sufficient stability of the experimental conditions during the measurement. The correctness of the value of the peak-broadening parameter ε used for the calculation of the ψ-scan simulations (Figs. 3*a*, 4*a*, 4*c* and 6*a*) is confirmed by the excellent agreement of the measured and calculated peak shapes of Figs. 6(*a*) and (*c*).

In Table 3 the unscaled observed structure factors

$$F_{obs}^{unsc} = \{I * A/[Lp * (1 + \alpha_{TDS})]\}^{1/2} \qquad (17)$$

of the 602, 0,1,12 and 061 reflections are given. I is the standardized integrated intensity, A is the absorption factor for spheres of Weber (1969) and Lp is the Lorentz–polarization factor as defined in (16*b*). The degree of polarization DP could not be measured during the experiment. At the five-circle diffractometer FICIDI (Wendschuh-Josties & Wulf, 1989) on beam line *D* at HASYLAB, DP varies between 85 and 95%, depending on the actual beam position. Therefore the mean, DP = 90%, was taken for the calculation of the values given in Table 3. The possible error of the structure factor due to this approximation is less than 1%. Correction for thermal diffuse scattering was applied using a modified version of the anisotropic one-phonon approximation (computer program *TDS2*) by Stevens (1974). The effect of extinction was ascertained to be less than 0·5% for the 602 reflection and was therefore neglected.

The differences in the unscaled observed structure factors obtained for the 602 reflection may be due to uncertainties introduced by standardization of the Bragg intensities. These uncertainties probably result from the inhomogeneity of the beam cross section,

Table 3. *Unscaled observed structure factors*

(*a*) Calculated from Bragg intensity of the possible reflections 602 and 0,1,12 and from *Unweganregung* intensity of the 'almost forbidden' 061 reflection
Pos. (Ref.): Reference position of the measurement; Pos. (Max.): position of peak maxima in Figs. 6(*b*) and (*c*); [a] and [b]: measurement before and after the ω–2θ–ψ scan, respectively

Possible reflections				'Almost forbidden' reflection 061			
				Pos.		Pos.	
h	*k*	*l*	F_{obs}^{unsc}	(Ref.)	F_{obs}^{unsc}	(Max.)	F_{obs}^{unsc}
6	0	2	80·15 (21)[a]	1	16·92 (22)	1	16·98 (31)
			83·76 (11)[b]		17·76 (20)	2	9·81 (32)
0	1	12	7·89 (63)[a]		17·55 (20)	4	9·31 (32)
			8·11 (75)[b]		17·36 (20)	5	4·69 (42)
			8·79 (44)[b]		17·58 (19)		

(*b*) Calculated from Bragg intensity of the 'almost forbidden' 061 reflection
Range: azimuthal angle range as indicated in Figs. 6(*c*) and (*d*); Num: number of scans used for calculation

Range	Num.	F_{obs}^{unsc}	Range	Num.	F_{obs}^{unsc}
A	101	1·56 (26)	*C*–*D*	181	1·50 (15)
B	101	1·66 (14)	*C*–*D*	161	1·49 (17)
C	241	1·45 (13)	*C*–*D*	141	1·49 (18)
C–*D*	221	1·49 (13)	*C*–*D*	121	1·45 (21)
C–*D*	201	1·51 (14)	*D*	101	1·45 (22)

the instability of the beam height and the varying tilt of the synchrotron radiation impinging on the sample and from the fact that with the monitoring device the intensity of the total beam cross section is measured, whereas the sample diffracts varying sections of this beam. The differences may be due also to the above-mentioned contamination of the second measurement by multiple-scattering events. The order of magnitude of this structure-factor fluctuation is consistent with previous experience of the authors on Bragg-intensity measurements at HASYLAB.

The 'structure factors' calculated from the *Umweganregung* intensity of the 061 reflection are also given in Table 3(*a*). The satisfactory agreement between the 'structure factors' evaluated for the repeatedly measured reference ω–2θ scans at position 1 of Figs. 6(*b*) and (*c*) demonstrates the excellent reproducibility of the diffractometer angle setting during the ω–2θ–ψ scan.

Whereas the four *Umweganregung* peaks are clearly visible in Figs. 6(*b*) and (*c*), no continuous Bragg-intensity peak is recognizable in Fig. 6(*b*). Since this intensity was expected to be at least twice as large as the intensity of the well resolved 0,1,12 reflection of Fig. 5, whose observed structure factor, given in Table 3(*a*), is comparable with the 'structure factors' of the *Umweganregung* peaks at positions 2 and 4 in Figs. 6(*b*) and (*c*), the 061 peak, expected by the M & L 79 model, should be significantly greater than for example the well resolved peak at ψ position 4 of Figs. 6(*b*) and (*c*). From inspection of Figs. 6(*b*) and (*c*) therefore this model can be rejected. The value for α_{33} given by M & L 79 and that given by M, J & K are far too large.

Because of the high background during the measurement, the intensity expected for the anharmonic parameters of Table 1 given by the authors is far too weak to be visible by inspection of Fig. 6(*b*). Improvement of counting statistics was achieved therefore by summing the intensities of individual ω-2θ scans in various azimuthal angle ranges indicated in Figs. 6(*c*) and (*d*). In Table 3(*b*) the corresponding structure factors of the 061 Bragg intensity are given. As can be seen from Fig. 6(*d*), the regions *A* and *B* are contaminated by very weak multiple-scattering events, whose 'structure factors' were calculated with the program *UMWEG* to be about two orders of magnitude smaller than the 'structure factor' of the peak at position 1 in Fig. 6(*c*). This explains the slightly higher values of the structure factors given in Table 3(*b*) for these regions. Only the region *C* is likewise free from very weak multiple-scattering events. The resulting ω-2θ scan, summed over the 241 individual scans measured in region *C*, is given in Fig. 7. To make sure that the integrated intensity calculated from the ω-2θ scans of region *C* was not influenced by the two peaks making the boundary of this ψ region, the evaluation of the integrated intensity was repeated for a decreasing number of ω-2θ scans in the middle part of the ψ region between the two *Umweganregung* peaks. The corresponding structure factors are also given in Table 3(*b*). Moreover, using Gauss functions for approximation of the *Umweganregung* peak shape, the possible resulting *Umweganregung* intensity in the part of the ψ region used for evaluation of the 061 Bragg intensity was estimated to be more than ten orders of magnitude smaller than in the maximum of the two neighbouring peaks, whereas the measured intensity in this region reached about 3% of these maxima. Therefore, it was concluded that the intensity obtained by the measurement was not due to multiple-scattering events.

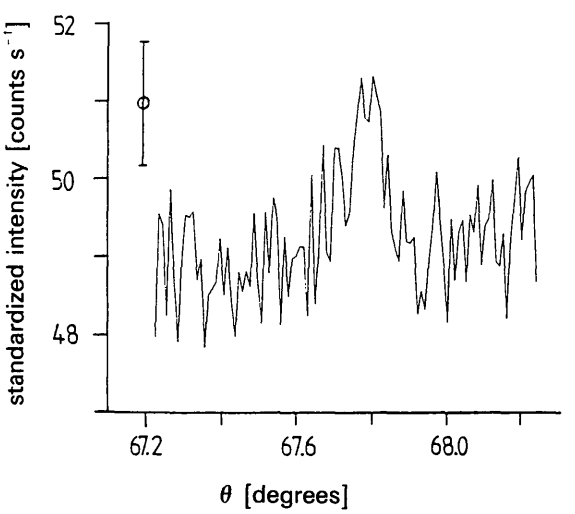

Fig. 7. The mean of the 241 measured ω-2θ scans of range *C*, standardized intensity *versus* ω.

Table 4. *Scaled observed and calculated structure factors*

(*a*) Comparison of M & L 79 and this work

	M & L 79		This work	
h k l	F_o	F_c	F_o	F_c
6 0 2	2·5735 (67)	2·5735	2·9074 (76)	2·9074
0 1 12	0·2652 (196)	0·0773	0·2996 (221)	0·2904
0 6 1	0·0475 (55)	0·3854	0·0537 (62)	0·0618

(*b*) Calculated structure factors as a function of the second-, third- and fourth-order anharmonic parameters. *F*1: calculated with M & L 79 fourth-order parameters; *F*2: calculated with authors' fourth-order parameters

		602		0,1,12		061	
α_{20}, β_{00}	α_{33}	*F*1	*F*2	*F*1	*F*2	*F*1	*F*2
M & L 79	−0·18	2·573	3·558	0·077	0·220	0·039	0·046
M & L 79	−1·80	2·573	3·558	0·077	0·220	0·385	0·455
Authors'	−0·18	1·775	2·907	0·136	0·290	0·049	0·062
Authors'	−1·80	1·775	2·907	0·136	0·290	0·489	0·616

In Table 4(*a*) the observed structure factors are compared with calculated ones. In the third and fifth columns, the parameters of M & L 79 and the authors' anharmonic parameters, respectively, were used for calculation of the structure factors. In the second and fourth columns the scaled observed structure factors, F_o, are given. In both cases the scale factor is fixed by the ratio of the observed and appropriate calculated structure factor of the 602 reflection. Because the second measurement of the 602 reflection was probably affected by multiple-diffraction events (Fig. 4*a*), the first measurement only was used for scaling. The mean values of the observed unscaled structure factors were used in the case of the 0,1,12 and 061 reflections in Table 4(*a*).

Apart from the fact that for the M & L 77 and 79 anharmonic parameters the truncated expansion [(11*b*)] of the anharmonic part of the thermal smearing function used in the OPP formalisms does not approximate the Boltzmann distribution function [(11*a*)] properly (Lüders & Rossmanith, 1988), these parameters moreover result in calculated structure factors for the very weak 0,1,12 reflection and the 'almost forbidden' 061 reflection, which are not consistent with the measured ones. From Tables 2(*a*) and (*b*) the 061 intensity was expected to be twice as large as the 0,1,12 intensity. In the M & L 79 anharmonic model the 'almost forbidden' 061 intensity should be five times as large as the weak 0,1,12 intensity, which is obviously in contradiction to the observation. On the other hand, the structure factors calculated with the authors' anharmonic parameters match the observed structure factors very well.

The dependence of the calculated structure factors on variations of the second-, third- and fourth-order anharmonic parameters respectively can be deduced

from Table 4(*b*). The 061 reflection is very sensitive to the third-order parameter and only weakly dependent on the fourth-order anharmonic parameters. On the contrary, because of its high l value, the 0,1,12 reflection strongly depends on the fourth-order parameters and is nearly independent of the third-order parameter. The far too small calculated structure factor of the 0,1,12 reflection in the M & L 79 model can therefore be attributed to the incorrect fourth-order parameters given in this model. This result confirms the statement by Rossmanith (1984) and Lüders & Rossmanith (1988) that the fourth-order anharmonic parameters given by M & L 79 are physically meaningless. The authors' fourth-order anharmonic parameters predict the 0,1,12 structure factor correctly. But, bearing in mind that, because of the strong correlation, the harmonic and fourth-order anharmonic parameters were not refined simultaneously and that the harmonic parameters evaluated using (13*a*) and (13*b*) probably include centrosymmetric anharmonic parts of the thermal motion, the physical interpretation of the fourth-order anharmonic parameters, derived by least-squares fit of measured Bragg intensity data sets, has to be considered with care. Furthermore, comparison of the 0,1,12 and 602 structure factors, calculated in the harmonic (Table 2*b*) and anharmonic approximation (Table 4*a*) using the authors' parameters indicate that the deviation from harmonic motion due to fourth-order anharmonicity is not significant.

As pointed out by Lüders & Rossmanith (1988), the series expansion in (11*b*) and the temperature factor in (12) may underestimate α_{33}. The small but significant intensity of the 061 reflection was therefore reanalysed, evaluating the temperature factor, *i.e.* the Fourier transform of the thermal smearing function t_j, given in (11*a*) by numerical integration, applying the method described by Lüders & Rossmanith (1988), as well as using (12). The results did not differ significantly, giving in both cases $\alpha_{33} = -0{\cdot}16\,(2) \times 10^{-19}\,\mathrm{J\,\AA^{-3}}$, indicating a small but significant antisymmetric anharmonic motion of the atoms in Zn.

The relatively high intensity of the 'almost forbidden' 301 and 303 reflections measured by M, J & K therefore cannot be due to anharmonic motion only. From (7) instead of (8) this intensity may be explained by static directional distortions of the electronic charge distribution associated with chemical bonding.

For simplicity of (2) to (10), the effect of anomalous dispersion has been neglected in this paper. As can easily be checked, all the conclusions remain valid if the anomalous dispersion is taken into consideration.

We are indebted to Professor Dr K. Hümmer and Dr E. Weckert for valuable support during the measurement on their ψ-(6-)circle diffractometer at HASYLAB, founded by the German Minister of Research and Technology (Förderkennzeichen: 05 463IXB). The authors' work was likewise founded by the German Minister of Research and Technology (Förderkennzeichen: 05 405IBB).

References

BUSING, W. R. & LEVY, H. A. (1967). *Acta Cryst.* **22**, 457-464.
DAWSON, B. (1967). *Proc. R. Soc. London Ser. A*, **298**, 255-263.
HÜMMER, K., WECKERT, E. & BONDZA, H. (1989). *Acta Cryst.* A**45**, 182-187.
International Tables for X-ray Crystallography (1974). Vol. IV. Birmingham: Kynoch Press. (Present distributor Kluwer Academic Publishers, Dordrecht.)
LÜDERS, H. & ROSSMANITH, E. (1988). *Acta Cryst.* A**44**, 554-558.
MERISALO, M., JÄRVINEN, M. & KURITTU, J. (1978). *Phys. Scr.* **17**, 23-25.
MERISALO, M. & LARSEN, K. (1977). *Acta Cryst.* A**33**, 351-354.
MERISALO, M. & LARSEN, K. (1979). *Acta Cryst.* A**35**, 325-327.
ROSSMANITH, E. (1984). *Acta Cryst.* B**40**, 244-249.
ROSSMANITH, E. (1985). *Z. Kristallogr.* **171**, 253-254.
ROSSMANITH, E. (1986). *Acta Cryst.* A**42**, 344-348.
ROSSMANITH, E., KUMPAT, G. & SCHULZ, A. (1990). *J. Appl. Cryst.* **23**, 99-104.
STEVENS, E. D. (1974). *Acta Cryst.* A**30**, 184-189.
WEBER, K. (1969). *Acta Cryst.* B**25**, 1174-1178.
WECKERT, E. (1988). *Zum Phasenproblem der Strukturanalyse.* Thesis, Univ. Erlangen-Nürnberg, Federal Republic of Germany.
WENDSCHUH-JOSTIES, M. & WULF, R. (1989). *J. Appl. Cryst.* **22**, 382-383.
WILLIS, B. T. M. & PRYOR, A. W. (1975). *Thermal Vibrations in Crystallography.* Cambridge Univ. Press.